Generic features of the primary relaxation in glass-forming materials

(Review Article)

Valery B. Kokshenev

Departamento de Fisica, Universidade Federal de Minas Gerais, Instituto de Ciências Exatas, Caixa Postal 702,
CEP 30123-970, Belo Horizonte, Brazil
E-mail: valery.kokshenev@gmail.com

We discuss structural relaxation in molecular and polymeric supercooled liquids, metallic alloys and orientational glass crystals. The study stresses especially the relationships between observables raised from underlying constraints imposed on degrees of freedom of vitrification systems. A self-consistent parametrization of the α-timescale on macroscopic level results in the material-and-model independent universal equation, relating three fundamental temperatures, characteristic of the primary relaxation, that is numerically proven in all studied glass formers. During the primary relaxation, the corresponding small and large mesoscopic clusters modify their size and structure in a self-similar way, regardless of underlying microscopic realizations. We show that cluster-shape similarity, instead of cluster-size fictive divergence, gives rise to universal features observed in primary relaxation. In all glass formers with structural disorder, including orientational-glass materials (with the exception of plastic crystals), structural relaxation is shown to be driven by local random fields. Within the dynamic stochastic approach, the universal subdiffusive dynamics corresponds to random walks on small and large fractals.

Contents

1. Introduction

Structural glass transformation in supercooled liquids is one of the long-standing fundamental problems of condensed matter physics. A process of glass creation is followed by the formation of intermediate metastable states in which a dramatic increase in viscosity and anomalous temperature behavior of transport characteristics is commonly studied above the *glass transformation temperature T_g* established by scanning calorimetry. An intriguing aspect of this process is the apparent connection between dynamics and thermodynamics [1].

There is great interest in complex studies, experimental and theoretical of the temperature-temporal behavior of primary structural relaxation in supercooled liquids (SCLs) and other glass formers. A wealth of *dynamic* data on relaxation *timescale* $\tau_T^{(\exp)}$, determined in viscoelastic, dielectric, conductivity, mechanical relaxation, light and neutron scattering experiments, is regarded as one of the main keys to the understanding of the problem of the structural glass transformation [1–4]. Instead of a unified approach to the problem given within one coherent framework, which is a challenge for theorists [1,4], in a number of mesoscopic-level descriptions was developed. They were worked out within the scope of the coupling [5,6], effective medium [7], percolation treatment [8], mesoscopic domain [9,10], trap diffusion [11], mobile defect [12], heterophase density fluctuations [13–15] and coarse-grained polymer-chain [4] models. In this review, the phenomenon of glass formation in liquids and solids is discussed on a mesoscopic scale of consideration with the elaboration for the percolative-geometric, kinetic-stochastic, and thermodynamic-statistic approaches. In the case of SCLs, the thermodynamic statistical consideration of the problem was introduced through cluster-size fluctuations [16] and in further developed within the heterostructured-cluster model [17] confronted with the percolation-type cluster treatment, earlier proposed in Ref. 18.

A structural relaxation process does not occur at a single temperature T_g, and at least two more *characteristic temperatures* are well distinguished in late-time, or slow relaxation. One of these is the *Vogel temperature T_0*, defined through the widely employed Vogel–Fulcher–Tammann (VFT) phenomenological form, which fits a temperature behavior of α-timescale $\tau_T^{(\exp)}$. Laying below T_g and being inaccessible in dynamical experiments, a fictive-divergence temperature T_0 signals a *dynamic instability* of the supercooled metastable state. Its physical meaning was recognized by many authors through the thermodynamic model by Adam and Gibbs (AG) [19]. According to this model, a description of metastable SCLs given in terms of the solid-like cooperatively rearranging regions (CRRs) displays an absolute *thermodynamic instability* at the Kauzmann temperature T_K [20]. Employing the idea of dynamic-thermodynamic correspondence, Richert and An-

gell have shown in [21] that the VFT form can be justified by the AG model, and thus a unique VFT-AG form can be introduced to fit simultaneously dynamic and thermodynamic data within a certain temperature domain, or *observation window*. In part, this finding is based on the relation between the "dynamic" and "thermodynamic" quantities: $T_0 = T_K$, established numerically [22–24] and analytically [25,26] in various glass formers.

The temperature observation window of the VFT-AG form, was shown [21] to be bounded from above by the α–β-relaxation bifurcation temperature, which in turn is often found to be close to the *crossover temperature T_c*, defined in the mode coupling theory (MCT) [3]. The existence of a material-independent boundary, considered as universal [27], was probably firstly predicted by Goldstein, as the lower limit for the free activated diffusion [28]. This surmise was brilliantly corroborated in experimental observations of break down of the Stokes–Einstein relation [29], α–β relaxation bifurcation [30], and Debye–Waller anomaly described in MCT at T_c [3,31]. The experimentally indicated temperature T_c was described by different authors as the VFT upper-domain temperature T_B [32,33], the viscosity-scaling upper-limit temperature T_C [34], the rotational-translational decoupling temperature T_c [29], the steepness-kink temperature T_c [17], as well as simply crossover temperature T_x [35–37].

In the idealized version of MCT, the dynamic instability at T_c is described by the algebraic-type divergence of the α-relaxation timescale. In the extended MCT, when additional relaxation channels, which are distinct from those provided by density fluctuations in SCLs, are taken into consideration [38], the divergence is avoided by turning it into as a smeared peculiarity. Anyway, according to MCT, the two distinct metastable states are distinguished in SCLs: the *moderately supercooled state*, in "weakly coupled fluids" [3] above T_c, and the *strongly supercooled state* in "strongly coupled fluids" [3] in deeply SCLs [1], below T_c. Employing the first-order temperature-derivative data on the α-relaxation timescale [32,33], these states were described near the kink in the timescale *steepness* [17]. We will show how the *timescale curvature* analysis provides further insights into the origin of underlying instabilities characteristic of both the supercooled states.

From the macroscopic point of view, no conceptual gap exists between spin glasses (metallic and non-metallic), orientational glasses (dipolar and quadrupolar), and structural (molecular and polymeric) glasses. A fruitful analogy between all three fields is constantly explored by researchers [25,36,39–44] and offers a theoretical basis for the development of generalized approaches. In our approach, a cooperative process of glass formation it treated in terms of material-abstract relaxing units, whose relaxation dynamics is controlled by short-range (intra-unit) and long-range (inter-unit) correlations. Such an approach can be thought as an ensemble of small and large solid-like clusters in

SCLs, earlier modelled, respectively, by isolated CRRs [19] and by coupling CRRs [5]. These clusters have no joint observable parameters. An alternative self-consistent description established within a minimum set of common parameters was proposed through the Gaussian statistics of CRRs in Refs. 16, 17.

In the present review we stress the relationships between thermodynamic and/or kinetic observable quantities, which are raised from underlying constraints imposed on degrees of freedom of the glass formation system. We especially focus on model and/or material independent relations. It will be shown that these macroscopic relations, established in the case of SCLs, also works well in other glass formers.

2. Timescale description

Below we discuss a set of static, kinetic, and thermodynamic macroscopically observable parameters, commonly involved in studies of the primary structural relaxation in glass formers. Also, additional auxiliary mesoscopic parameters are introduced in order to establish relations between observables in a certain closed form.

2.1. Vogel–Fulcher–Tammann form

During the glass transformation, structural relaxation does not occur at a single temperature T_g, as well as the underlying mechanism is not described by a single kinetic-thermodynamic parameter, such as the fragility m_g. A minimum set of parameters should, at least, be extended by the crossover temperature T_c and the corresponding slowing-down dynamical exponent γ_c. These and other related to them parameters can be introduced through the "dynamical" scaling VFT form and then specified by the "thermodynamic" AG model.

The phenomenological VFT fitting form, namely

$$\tau_T^{(VFT)} = \tau_{\min}^{(VFT)} \exp\left(\frac{DT_0}{T-T_0} \right), \qquad (1)$$

which also reads as

$$\log_{10}\tau_T^{(VFT)} = \log_{10}\tau_{\min}^{(VFT)} + \frac{B}{T-T_0}, \quad \text{with} \quad B = \frac{DT_0}{\ln 10}, \quad (2)$$

is widely used to describe the non-Arrhenius behavior of the structural relaxation observed in amorphous liquids and solids. Proposed in the 1920s, it performs well within the temperature range, established approximately as $T_g \leq T < T_c$, which in SCLs corresponds to the relaxation time $10^{-7\pm1} < \tau_T^{(\exp)}/s \leq 10^{2\pm1}$ and to the shear viscosity between $10^{4\pm1}$ and $10^{13\pm1}$ Poise. Apparently, a pre-factor $\tau_{\min}^{(\exp)} = 10^{-14\pm2}$ s reflects the Debye molecule vibrational times, characteristic of the normal-liquid (NL) thermodynamically stable state, which follows the standard Arrhenius-form description. The physical meaning of the Vogel

temperature T_0 is ensured by the underlying low-temperature (LT) asymptotic instability of the supercooled metastable state. Its origin was elucidated within the framework of a microscopic defect-aggregation model [39], supported by pressure-dependent experiments [12].

The physical meaning of the Vogel temperature T_0 is ensured by the underlying LT asymptotic instability of the supercooled metastable state. Its origin was elucidated within the framework of a microscopic defect-aggregation model [39], supported by pressure-dependent experiments [12].

2.2. Adam and Gibbs model

In the thermodynamic AG model, the kinetic properties of SCLs are described [19] by

$$\tau_T^{(AG)} = \tau_{\min}^{(AG)} \exp\left(\frac{\Delta\mu^{(AG)} n_T}{k_B T} \right), \qquad (3)$$

obtained through the average *transition probability* $1/\tau_T^{(AG)}$ of the smallest-size CRRs. Here $\Delta\mu^{(AG)}$ is the molar (solid-over-liquid excess) chemical potential, approximated by a constant, whereas n_T stands for the mean number of molecules which constitute the rearranging region. Equation (3) was deduced from thermodynamic consideration, given by

$$\log_{10}\tau_T^{(AG)} = A + \frac{C}{T\Delta S_T^{(AG)}}, \quad \text{with} \quad \frac{C}{\Delta S_T^{(AG)}} = \frac{\Delta\mu^{(AG)} n_T}{k_B \ln 10}, \qquad (4)$$

where $\Delta S_T^{(AG)}$ is the molar *configurational entropy* defined as the excess liquid-over-solid entropy in the SCL molecular system.

2.3. Mode coupling theory scaling

An application of the MCT algebraic-type scaling, namely

$$\tau_T^{(MCT)} = \tau_{\min}^{(MCT)} \left(\frac{T_c}{T-T_c} \right)^{\gamma_c}, \quad \text{for} \quad T_c < T_y \leq T < T_A, \quad (5)$$

is limited by the Arrhenius crossover temperature T_A, below which the appearance of the SCL state is signaled by a deviation from the standard Arrhenius behavior [3,32]. The temperature domain of the MCT fitting form (5) was revealed in SCLs through the temperature-derivative analysis in Ref. 30. It was approximated by $T_B < T < T_A$, where T_A is the Arrhenius crossover temperature and T_B is the α–β-relaxation bifurcation temperature [30]; T_y in Eq. (5) designates the lowest temperature at which the algebraic MCT form fits experimental data. The *slowing-down exponent* γ_c, defined in Eq. (5), is rather sensitive to the location of T_c as well as to the temperature region of the fitting experimental curve [3,32,33,40,45]. In general, the fitting data established through Eq. (5) are in the range $2 \leq \gamma_c^{(\exp)} < 3$ for glass-forming liquids and $3 \leq \gamma_c^{(\exp)} < 4$ for polymers.
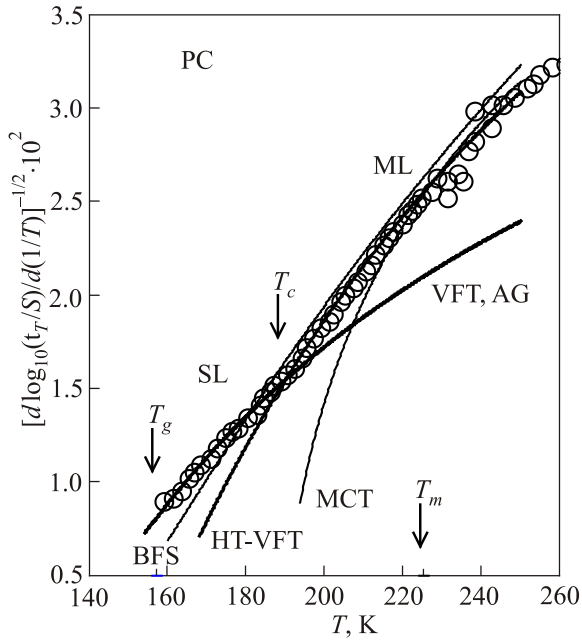
Fig. 1. Comparative analysis of the different fitting forms suggested for the primary time relaxation scale: the first-order timescale derivative function versus temperature in propylene carbonate. Points: dielectric and dc conductivity relaxation data $\tau_T^{(exp)}$ reproduced from Fig. 12 in Ref. 33. The phenomenological Vogel–Fulcher–Tammann form is presented by VFT and HT-VFT lines corresponding to Eq. (2) given with, respectively, $T_0 = 132$ K, $B = 389$ K and $T_0^{(HT)} = 153$ K, $B^{(HT)} = 158$ K. The AG model is given through Eq. (4) adjusted with Eq. (2) and the VFT line. The MCT fitting is obtained through Eq. (5) with $T_c = 176$ K and $\gamma_c = 2.7$. The metastable moderately (ML) and strongly super-cooled-liquid (SL) states are shown. The arrows indicate the characteristic temperatures for structural glass transformation.

With the aim of illustrating the effectiveness of the discussed fitting forms, in Fig. 1 we extend the timescale temperature-derivative analysis proposed for propylene carbonate by Stickel *et al.* in Refs. 32, 33.

The characteristic temperatures and other macroscopic parameters commonly employed for the timescale description of glass-forming molecular organic and polymeric liquids are accumulated, respectively, in Tables I and II in Ref. 46.

2.4. Observation windows

As seen in Fig. 1, the two distinct SCL states are experimentally observed through the temperature windows, established by the thermodynamic-dynamical parameters T_0, T_g, and T_c described, respectively, with the help of the VFT and MCT timescale fitting forms. Being rather close in the fragile glass formers and relatively distant in the strong glass formers, these crossover-state temperatures are strongly material dependent. In contrast, the corresponding *temporal* observation windows, established by the "almost" material-independent characteristic times [27,47] $\tau_c^* = 10^{-7\pm1}$ s and $\tau_g^* = 10^{2\pm1}$ s, are wide and model-independent. In what fol-

lows, a connection between the temperature and temporal SCL-state windows is quantified through the material-dependent fragility. This analysis yields a universal constraint equation imposed on the characteristic temperatures.

2.5. VFT equation

The strength parameter D defined in Eq. (1) presumably does not depend on temperature. As a matter of fact, this condition cannot be satisfied when the VFT form is applied to a wide temperature range. An example is that of ortho-terphenyl (OTP), where the LT fitting within the temperature range $T_g \leq T \leq T_c$ gives $T_0 = 200$ K and $D = 10.4$, and the high-temperature (HT) fitting ($1.1 T_g \leq T \leq 1.8 T_c$) requires $T_0 = 231$ K and $D = 2.98$ (see Fig. 2 and Table 1 in Ref. 45).

In view of the qualitative findings in Refs. 3, 21, 32, 33 obtained through the VFT form for SCLs, we rewrite Eq. (1) with taking into consideration its validity domain laying beyond the SL state, namely

$$\tau_T^{(VFT)} = \tau_{min}^{(VFT)} \exp\left(\frac{D_g}{\varepsilon_T}\right), \text{ with } \varepsilon_T = \frac{T}{T_0} - 1, \text{ for } T_0 < T < T_c,$$

(6)

and refer to it as the VFT *equation*, given in terms of the auxiliary function ε_T. As has been shown in [48], the *strength index* $D_g = m_{g\,min}\varepsilon_g \ln 10$, and the lower fragility limit $m_{g\,min} \approx 16$ for a bulk of glass-forming materials was also established [49].

In order to characterize the timescale temperature behavior, we define, in the spirit of Ref. 50, the *timescale steepness function*, namely

$$m_T \equiv -\frac{d\log_{10}\tau_T}{d\ln T} = -\frac{T}{\ln 10}\frac{d\ln \tau_T}{dT}.$$

(7)

Applying it to Eq. (6), one has for the VFT timescale steepness

$$m_T^{(VFT)} = \frac{D_g}{\ln 10}\frac{1}{\varepsilon_T}\left(1 + \frac{1}{\varepsilon_T}\right) = \frac{D_g}{\ln 10}\frac{TT_0}{(T - T_0)^2},$$

(8)

which at $T = T_g$ naturally gives the glass-former fragility [48]

$$m_g = m_g^*\left(1 + \frac{1}{\varepsilon_g}\right) = \frac{m_g^*}{1 - T_0/T_g}.$$

(9)

The material-independent lower limit fragility $m_g^* \equiv m_{min}$, namely

$$m_g^* = m_g^{*(VFT)} = m_{g\,min} = \frac{D_g}{\ln 10}\frac{1}{\varepsilon_g}, \quad \varepsilon_g = \frac{T_g}{T_0} - 1$$

(10)

follows from the VFT equation (6), though it can be also given in the *model-independent* form as

$$m_g^* = \log_{10}\left[\frac{\tau_g^{(exp)}}{\tau_\infty^{(exp)}}\right].$$
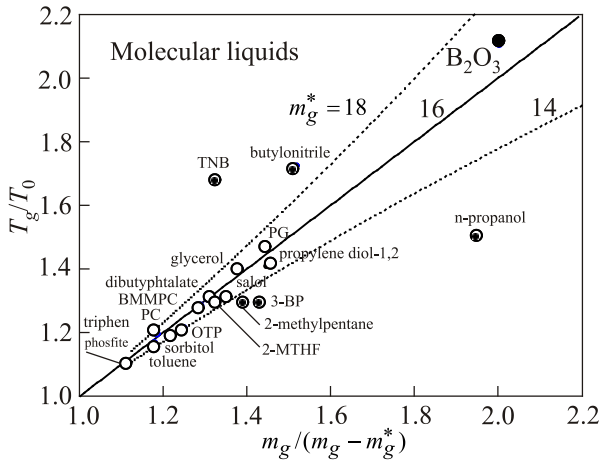
(11)

Fig. 2. Observation of the characteristic-temperature constraint T_g/T_0 in SCL molecular organic liquids extended by inorganic boron trioxide (B_2O_3). Points are estimated with the help of Table I in Ref. 46 and given only in those cases for which the whole VFT experimental set on T_g, T_0, and m_g is available. The solid line corresponds to Eq. (12) with $m_g^* = 16$, and the dotted lines show the typical experimental scatter given by $m_g^* = 14$ and 18. The dots in the circles indicate the cases exceeding the typical error.

Indeed, even Eq. (11) is a consequence of Eq. (10), and can be tested by Eqs. (6) and (8), taken at T_g, it does not depend on any specific VFT-form characteristics. The insertion the estimates $\tau_g^{(exp)} = 10^{2\pm1}$ s and $\tau_\infty^{(exp)} = 10^{-14\pm2}$ s in Eqs. (9) and (11) yields the well known constraint for the characteristic-temperature ratio [48,51]

$$\frac{T_g}{T_0} = \frac{m_g}{m_g - m_g^*}, \qquad m_g^* = 16 \pm 2. \qquad (12)$$

The experimental validity of Eq. (12) for SCLs is tested in Fig. 2.

As can be deduced from Fig. 2, the major part of SCLs are captured in their SL state by the VFT equation, bounded by the characteristic temperatures T_0 and T_g. Formally, the constraint observed in Fig. 2 is a consequence of the consistency condition of the SL-state description made through the timescale and its steepness and revealed at T_g. Physically, it signals the presence of the unique material-independent mechanism for the primary relaxation in SCLs. The same can be stated in relation to glass-forming polymers and metallic alloys, where Eq. (12) works well, as shown in Refs. 47 and 52, respectively. The deviations indicated in Fig. 2 by the dots placed into the circles are associated with the inadequate application of the VFT form (2), revealed through the fit-parameter inconsistency.

2.6. HT-VFT approach

Qualitatively, the SL and ML states can be thought of as self-similar metastable states, which during solidification exhibit well distinguished geometrical, kinetic, and thermo-

dynamic features. They are commonly studied at the glass-transformation characteristic temperatures, which establish the observation windows given by, respectively, $T_g \leq T < T_c$ and $T_c \leq T < T_A$, and can be mapped to the timescale windows via $\tau_g^* \geq \tau_T^{(SL)} > \tau_c^*$ and $\tau_c^* \geq \tau_T^{(ML)} > \tau_A$.

Searching for the simplest description, we employ the VFT and HT-VFT forms, introduced by the corresponding Vogel temperatures T_0 and $T_0^{(HT)}$. Taking into consideration the experimental fact that $T_0^{(HT)} \approx T_g$, established for SCLs [21,33], one notes that the parameters T_0 and T_g in the SL state play the role similarly to T_g and T_c, in the case of the ML state. Indeed, the temperatures T_0 and T_g are close to the *critical* temperatures where the *global* thermo-dynamic (Kauzmann) and dynamic (Gaussian) [16,53] instabilities are expected; whereas T_g and T_c are the local-instability (crossover) temperatures at which SL and ML states rebuild. These introduce the critical-point and cross-over-point similarities existing between SL and ML states described through the VFT and HT-VFT forms. As a consequence, the timescale steepness function, given in Eq. (9) for the SL state at T_g, can be immediately rewritten for the ML case at T_c as

$$m_c = m_c^* \left(1 + \frac{1}{\tilde{\varepsilon}_c}\right), \text{ with } \tilde{\varepsilon}_c = \frac{T_c}{T_g} - 1. \qquad (13)$$

The material-and-model-independent lower fragility limit

$$m_c^* = m_{c\,min} = \log_{10}\left(\frac{\tau_c^{(exp)}}{\tau_{min}^{(exp)}}\right) = 7 \pm 1 \qquad (14)$$

in the ML state was numerically established [47] through the experimental relaxation time $\tau_c^{(exp)} \equiv \tau_c^* = 10^{-7\pm1}$ s. Independently, τ_c^* was found as a "magical" relaxation time [27], attributed to a hopping relaxation mechanism of the elementary SCL excitations discussed in Ref. 54.

In the absence of experimental data on the ML-state fragility at T_c, one needs to connect m_c with m_g. Keeping this in mind, we treat the steepness function m_T as a piece-wise smooth function extrapolated to the HT range $T_g + 0 \leq T \leq T_c - 0$ and apply the Taylor series. This results in $m_g = m_c + (T_g - T_c)m_{T=T_c}'$, which in combination with $m_{T=T_c}' = -m_c/\tilde{\varepsilon}_c T_c$ following from Eq. (13) and m_c given in Eq. (13) provides the desirable relation $m_g = m_c^*(1 + 2/\varepsilon_c)$. This yields the ratio [47]

$$\frac{T_c}{T_g} = \frac{m_g + m_c^*}{m_g - m_c^*}, \quad m_c^* = 7 \pm 1, \qquad (15)$$

with the ML lower fragility limit m_c^* established in Eq. (14). In Fig. 3 we give numerical analysis of the obtained ratio T_c/T_g for liquid and solid glass-forming materials.

Bearing in mind the analyses presented in Figs. 2 and 3, the hypothesis on the existence of the critical-and-crossover point similarity in SCLs can now be extended to
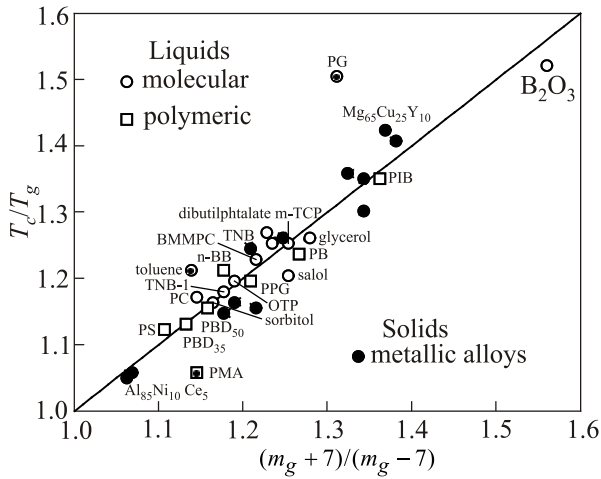
Fig. 3. Experimental testing of the characteristic-temperature constraint T_c/T_g in distinct glass-former materials. Open circles and squares are available experimental data for molecular liquids and polymers chosen, respectively, from Tables I and II in Ref. 46. The data marked by solid points indicate those which exceed the typical experimental error established in Eq. (14). The closed circles are data for 12 structurally disordered metallic alloys taken from Table I in Ref. 52. The solid line corresponds to Eq. (15) with $m_c^* = 7$.

all structurally disordered glass formers. With the help of Eqs. (12) and (15), it is quantified by the useful equations

$$m_g = \frac{m_g^*}{1 - T_0/T_g} = m_c^* \frac{T_c/T_g + 1}{T_c/T_g - 1}. \qquad (16)$$

2.7. Universal equations

As seen from Eqs. (16), the glass-transformation characteristic temperatures are not independent. When one excludes m_g from the constraints (16), the following material-independent, universal *characteristic-temperature equation* (CTE), namely

$$\frac{T_c}{T_g} = \frac{T_g\left(\frac{m_g^*}{m_c^*} + 1\right) - T_0}{T_g\left(\frac{m_g^*}{m_c^*} - 1\right) + T_0}, \qquad (17)$$

can be obtained. Numerically, Eq. (17) is close to the interpolative solution

$$\frac{T_c}{T_g} - \sqrt{\frac{T_g}{T_0} - \frac{3}{4}} - \frac{1}{2} = 0 \qquad (18)$$

deduced [47] from Eqs. (16) under the simplified condition $m_g^*/m_c^* = 2$. One can see that both Eqs. (17) and (18) satisfy the case of the *ideal* glass transition introduced by a single transition temperature $T_0 = T_g = T_c$.

Other forms of the universal CTE were also proposed. By application of the Lindeman melting criterion for SCL solid-like clusters, Novikov *et al.* in Ref. 55 obtained the CTE in the "square-root" form $T_g = \sqrt{T_0 T_c}$, which is shown [47] the lower limit of the "exact" Eq. (17), i.e., $T_{g\,min} = \sqrt{T_0 T_c}$. The upper limit was found [47] in the "cubic-root" form $T_{g\,max} = \sqrt[3]{T_0 T_c^2}$.

In Ref. 25, Odagaki developed a controlled-diffusion approach to the primary relaxation. By applying the AG model [19] he came to the equations under interest, which can be represented here in the following two equivalent forms, namely

$$\frac{T_g}{T_c} = \frac{1}{2}\left(1 + \frac{T_0}{T_c}\right), \text{ or } \frac{T_c - T_0}{T_c - T_g} = 2. \qquad (19)$$

One can see that these forms satisfy the ideal-glass transition condition. Remarkably, Eq. (19) was re-derived by Mohanty *et al.* [26] without recourse to the AG model. Numerical analysis of the universal CTEs is given in Fig. 4.

The choice of substances in Fig. 4 is limited by the availability of the complete set of experimental characteristic temperatures. The best fitting of experimental data on SCLs and glass-forming polymers was achieved for the fitting parameter $m_g^*/m_c^* = 2.22$ and 2.27, respectively (see also analysis in Ref. 17). The case of metallic alloys with the fitting parameter 2.17 is shown in Fig. 4. The Odagaki CTE (19) numerically corresponds to the ratio $m_g^*/m_c^* = 2.45 \pm 0.10$. As seen, in all of the cases considered here the fitting parameter does not exceed the domain established by $m_g^*/m_c^* = 2.3 \pm 0.3$, which also includes a scatter of the experimental data given in Eqs. (12) and (14).
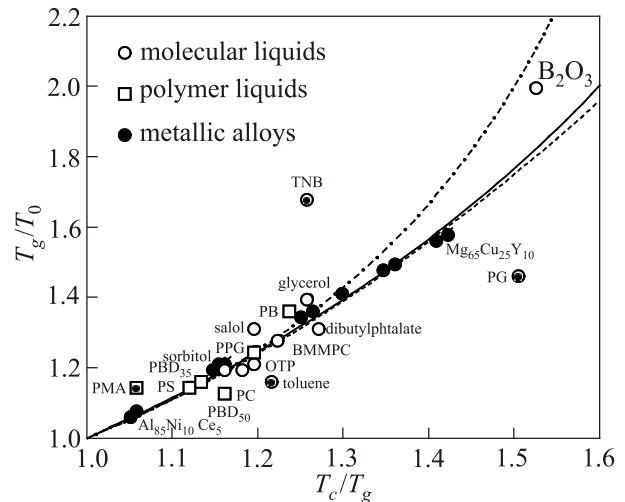

Fig. 4. Universal equations for the glass-transformation characteristic temperatures. Symbols are described in Fig. 3. The solid line is given by Eq. (17) with the material-independent parameter $m_g^*/m_c^* = 2.17$. The dashed and dashed-dotted lines are drawn through Eqs. (18) and (19), respectively.

3. Stochastic dynamic description

Besides non-Arrhenius behavior, the non-Debye temporal decay of structural correlations is a generic feature of collective relaxation dynamics of all glass formers in supercooled states. In other words, the observed late-time dynamic relaxation is substantially non-exponential, at least near T_g. The dynamic response function is commonly fitted by the two temperature-dependent parameters β_T and τ_T attributed to the phenomenological Kohlrausch–Williams–Watts (KWW) form. In contrast, the short-time asymptote of the primary relaxation exhibits an algebraic-type temporal behavior, which is studied [3] through the von Schweidler scaling law parametrized by the dynamical exponent b_T. A general question arises: can this small set of observable dynamical parameters definitively identify the underlying mechanisms for structural (and orientational) relaxations in microscopically distinct materials? This is a permanent challenge to any microscopic approach.

3.1. Random walks

In [56] we have provided a geometric interpretation of structural glass transformation in terms of late-time surviving percolation clusters, which were introduced through the exponentially small probability of their volume-size distribution. In what follows, we improve our study of the primary relaxation dynamics by taking into account the slow part of structural rearrangements and emphasizing the identification of relaxation mechanisms.

A cooperative dynamics of self-similar relaxing units (Debye-type clusters) in the formation of the metastable supercooled state can be treated as a diffusion process on fractals realized by a random walker (RW). At a given T, the mean-square deviation of the *diffusion* length R, accounted from the zero starting point, is described by

$$\left\langle R^2 \right\rangle_{RW} = R_T^2 \sim \tau_{DT}^{2/z}, \quad \left\langle ... \right\rangle_{RW} = \int_0^\infty ... P_T^{(RW)}(x)dx,$$

$$\text{and} \quad x = \frac{R}{R_T}, \tag{1}$$

where $\left\langle ... \right\rangle_{RW}$ stands for the effective-medium configurational average. This equation represents a *dynamic scaling hypothesis*, firstly proposed by Halperin and Hohenberg for thermal transitions [57]. Instead of the mean percolation cluster size (see Eq. (1) in [18]), R_T is introduced here as the square-root mean size of the region explored by RW. Besides the asymptotically large ($R \gg R_T$) percolative clusters, the asymptotically *small* RW clusters will be taken into account on the mesoscopic scale of consideration. Their random size R, namely

$$R_a \ll R \ll R_T, \tag{21}$$

is bounded by the lower (upper) limit of the mesoscopic (microscopic) scale, discussed in [19,56], as well as by the characteristic *correlation length* R_T, which is the upper limit of the domain of the intrinsic-cluster similarity or self-similarity [58].

Following the idea of the phase-ordering kinetics [59], we employ [18] the *dynamic scaling law*

$$\tau_D(R) = \tau_{DT} \left(\frac{R}{R_T} \right)^{z_g}, \quad \text{with} \quad R_T \geq R_a, \tag{22}$$

introduced near T_g with the help of the dynamical RW *diffusion exponent* z_T and restricted by the minimum cluster size R_a. Alternatively, the *cluster-growth dimension* can be defined as

$$z_g = \frac{d \ln \tau_D(R)}{d \ln R} = \left(\frac{d \ln \tau_{DT}}{d \ln R_T} \right)_{T=T_g}, \tag{23}$$

on the basis of the random and mean relaxation times attributed to self-similar clusters.

3.2. Relaxation functions

For the analysis of the *relaxation function* $\varphi^{(\exp)}(t,T)$ observed in dielectric spectroscopy, the overall-frequency Cole–Davidson fitting form is generally used [3]. Meanwhile, the slow part of the asymmetric α-relaxation function is fitted by the KWW form, given by late-time (low-frequency) asymptote of $\varphi^{(\exp)}(t,T)$, which at a fixed temperature T, close to T_g, can be given as

$$\varphi_S^{(\exp)}(t,T) \propto \exp\left[-\left(\frac{t}{\tau_T} \right)^{\beta_g} \right], \quad \text{for } t \gg \tau_g. \tag{24}$$

Here β_g is the Kohlrausch or *stretching exponent*, which commonly weakly depends on T, in the vicinity of T_g. The corresponding fast part is prescribed by the von Schweidler scaling law, namely

$$\varphi_F^{(\exp)}(t,T) \propto 1 - B\left(\frac{t}{\tau_T} \right)^{b_g}, \quad \text{for } t \ll \tau_g, \tag{25}$$

controlled by the exponent b_T at $T \approx T_g$, with $0 < b_T < 1$. For many relaxation processes, Eq. (25) can be extended for a period of over two decades [3]. The process of glass formation is followed by the strengthening of dynamic correlations. As the temperature approaches T_g from above, it evolves smoothly, starting from the Debye behavior, typical of the normal liquid state [8,10,60]. The relaxation function can be therefore approximated by the ensemble of modified Debye-type clusters. Such kind of percolation clusters was shown [56] to be distinct from those employed in the standard percolation theories [61,62], earlier developed as geometrical version of the order-disorder transitions. The trial ensemble of dynamically stable Debye

clusters of random radius-size R relaxing with time $\tau_D(R)$ is introduced in Eq. (20). Thus, $\varphi_T(t)$ gradually changes from the HT Debye form to that given as

$$\varphi_{S,F}^{(mod)}(t,T) = \int_0^\infty \exp\left[-\frac{t}{\tau_D(R)}\right] P_T^{(RW)}(x)\,dx. \quad (26)$$

The mechanism for stabilization of long-living correlated regions is therefore specified by the their radius-distribution probability density $P_T^{(RW)}(x)$ introduced in Eq. (20). For example, the trivial case of the Brownian dynamics ($z=2$) is given by RWs driving by the Gaussian distribution $\sqrt{\pi/2}\exp(-x^2/2)$, with $x = R/\tau_{DT}D_B$, where D_B is the Brownian diffusion constant. In real vitreous relaxation phenomena with underlying *anomalous diffusion motion* of atoms, defects, and charges or excitations, the dynamical exponent $z > 2$, because many neighbors of each step of RW are unavailable, and the walker is obliged to return into direction of his starting point [58]. These physical situations are going to be analyzed within the frameworks of restricted-diffusion models [63].

In [63], Zumofen, Klafter and Blumen re-examined, analytically and numerically, three well known theoretical models, elaborated to describe (i) random walks directed by random fields, (ii) dispersive motion due to continuous time random walks, and (iii) random walks on regular fractals. It has been established that for incoherent and dissipative motion in disordered systems, where the anomalous diffusion is well pronounced, the RW distribution $P_T^{(RW)}$ (20) does not deviate significantly from the Gaussian [63]. We therefore represent it here in a generalized *pseudo-Gaussian* zero-centred normalized form

$$P_T^{(RW)}(x) = Cx^g\exp(-cx^h), \text{ with } C = \frac{c^{\frac{1+g}{h}}}{\Gamma\left(\frac{1+g}{h}\right)}h, \quad (27)$$

where $\Gamma(y)$ is the Gamma function. The cluster-shape parameters g and h are not independent constants. They differ for mesoscopically large ($x>1$) and small ($x<1$) clusters, but their typical lower bounds are [63]: $c>0$, $g>-1$, and $h>1$.

Both the slow-regime (24) and fast-regime (25) relaxation functions have been analyzed through Eq. (26), where the distribution function is given in Eq. (27). They are found through the method of steepness descent presented as

$$\varphi_{S,F}^{(mod)}(t,T) \sim \int_0^\infty \exp\left[-\psi_\lambda(x)\right]d\xi \propto \frac{\exp\left[-\psi_\lambda(x_0)\right]}{\sqrt{\psi_\lambda''(x_0)}}, \quad (28)$$

following from Eqs. (26) and (28) with the help of the auxiliary function $\psi(\lambda,x) = \lambda x^{-z} + cx^h - g\ln(x)$. A straightforward estimation gives

$$\varphi_{S,F}^{(RW)}(t,T) \propto C\sqrt{\frac{\pi}{2}}\left[1+\mathrm{erf}\left(\sqrt{\frac{x_0^2\psi_0''}{2}}\right)\right]\frac{\exp(-\psi_0)}{\sqrt{\psi_0}}, \quad (29)$$

where $\mathrm{erf}(y)$ is the standard error function. The saddle points x_0 are given by the roots of equation $\lambda z x_0^{-z} - chx_0^h + g = 0$. They also satisfy the stability condition $\psi_0'' = czh(1+\frac{h}{z})x_s^{h-2} - zgx_s^{-2} > 0$. The result is presented in the two-regime asymptotic form

$$\varphi_{S,F}^{(RW)}(t,T) \propto \frac{C}{\sqrt{z}}\frac{x_0^{1+g}\exp\left[-c(1+\frac{h}{z})x_0^h\right]}{\left[c(1+\frac{h}{z})x_0^h - g\right]^{\frac{1}{2}}}, \quad (30)$$

where the corrections are exponentially small, in the case of the slow KWW regime, or algebraically small, in the fast von Schweidler regime. The two distinct asymptotes are associated with metastable large clusters introduced by

$$x_{0S} = \left(\frac{t}{\tau_{DT}}\frac{z_g}{c_S h_S}\right)^{\frac{1}{z_g+h_S}}; \quad (31)$$

and with the small clusters given by

$$x_{0F} = \left(\frac{t}{\tau_{DT}}\frac{z_g}{|g_F|}\right)^{\frac{1}{z_g}}, \text{ if } g_F \neq 0,$$

$$\text{otherwise, } x_{0F} = \left(\frac{t}{\tau_{DT}}\frac{z_g}{c_F h_F}\right)^{\frac{1}{z_g+h_F}}. \quad (32)$$

Finally, a comparison of $\varphi_S^{(RW)}(t,T)$ with the late-time observed asymptote (24), and of $\varphi_F^{(RW)}(t,T)$ with the short-time asymptote (25), represented in the interpolation form $\exp[-B(t/\tau_T)^{b_g}]$, provides predictions for the dynamical exponents, namely

$$\beta_g^{(RW)} = \frac{h_S}{z_g+h_S} \text{ and } b_g^{(RW)} = \frac{h_F}{z_g+h_F}. \quad (33)$$

The observed primary relaxation time

$$\tau_T = \tau_{DT}c_S^{-\left(\frac{1}{\beta_g}-1\right)}\beta_g^{\frac{1}{\beta_g}-1}(1-\beta_g) \quad (34)$$

emerges naturally as the properly renormalized Debye-cluster relaxation time τ_{DT}.

Before starting a discussion about conceivable relaxation mechanisms, one needs to make an appropriate choice for the model parameters h_S and h_F in Eq. (33). These parameters play the role of effective space relaxation dimensions d_S and d_F for, respectively, large and small

clusters discussed in [56]. In general, geometrically similar RW clusters fall into distinct dynamic regimes, which known classification is far from exhaustive. The three typical examples are specified in Table 1.

As seen in Table 1, the large-cluster distribution parameters obey Fisher's cluster (size-and-shape) relation [64]

$$h_S = \frac{z}{z-1}, \tag{35}$$

tested [63] analytically and numerically for the CTRW and RWF models. A question arises as to whether Eq. (35) is consistent with the experimental observation of the KWW exponent β_g predicted in Eq. (33). If one excludes h_S from a couple of Eqs. (33) and (35) and putts $z = z_g$, he obtains $z_g \beta_g = 1$ for Fisher's constraint (35). Restricting our consideration by the subdiffusive case $z_g > 2$, one has the model constraints $\beta_g^{(CTRW)}$, $\beta_g^{(RWF)} < 1/2$ that makes the fractal-time (CTRW) and the fractal-space (RWF) models inappropriate for SCLs in which $\beta_g^{(liq)} \geq 0.5$, as follows from experimental data shown in Fig. 1 in [56].

Equations (33) provide predictions for the subdiffusive primary relaxation, namely

$$z^{(DRW)} = h_S^{(DRW)}\left(\frac{1}{\beta}-1\right) = 2\left(\frac{1}{b}-1\right). \tag{36}$$

These equations were used near T_c in [65] for describing of the dielectric loss spectrum observed via the MCT scaling forms.

Table I. Parameters for the RW propagator function (27) established [63] through the three fundamental models of anomalous diffusion

Models	g_S	h_S	g_F	h_F	Dimensions
DRW	0	$>2.5^{(a)}$	0	$2.0^{(a)}$	$d = d_f+1,$ $d_f = 1$
CTRW	$-\dfrac{z-2}{2(z-1)}$	$\dfrac{z}{z-1}$	<0	>0	$d = d_f = 1$
RWF	$\dfrac{2d_f-z}{2(z-1)}$	$\dfrac{z}{z-1}$	0	z	$d_f < z$

Abbreviations: DRW — directed random walks in one-dimension random transverse field; CTRW — continuous-time random walks, RWF — random walks on fractals such as Sierpinski gaskets.

Notations: g, h are the cluster-shape parameters designated by indexes S and F for, respectively, slow and fast regimes; d, d_f, and z are dimensions for, respectively, Euclidean, fractal, and RW cluster spaces. $^{(a)}$The given (large and small) cluster limit asymptotic ($x \to \infty$, $t \to \infty$, and $x \to 0$) parameters are derived from the numerical experimental data shown in Fig. 8.14 in Ref. 63.

Also, a relation between the primary relaxation time and the *mean* intrinsic time of solid-like Debye clusters

$$\tau_T = \tau_{DT}\beta_g(1-\beta_g)^{1/\beta_g-1} \tag{37}$$

follows from the simplest model (28), where τ_T and β_g can be observed by means of the KWW fitting form.

3.3. Non-Debye versus non-Arrhenius behavior

Using Eq. (22) in the scaling form $\tau_{DT} = \tau_a(R_T/R_a)^{z_g}$, and taking into account Eq. (37), we estimate the timescale steepness (7) at T_g, namely

$$m_g = m_z^* z_g \text{ with } m_z^* = -\left(\frac{d\log_{10}R_T}{d\ln T}\right)_{T=T_g}. \tag{38}$$

This provides a link between the fragility and the cluster-dimension dynamical exponent (23). Furthermore, one obtains the dynamical relation

$$m_g = m_\beta^*\left(\frac{1}{\beta_g}-1\right), \text{ with } m_\beta^* = m_z^* d_g, \tag{39}$$

which can be read as a model prediction for the stretching exponent

$$\beta_g = \frac{m_\beta^*}{m_g + m_\beta^*}. \tag{40}$$

3.4. Diffusive mechanisms in polymers

In Fig. 5, the DRW model (36) is tested through the KWW relaxation observed in glass-forming polymers.

As seen in Fig. 5, scantiness and uncertainty of the available experimental data do not allow to make a choice between the two proposed alternatives. One of them is the DRW model, and another is the coupling model by Ngai [6], which prediction coincides with that of the defect diffusion model (DDM) [68], initially proposed in Ref. 39. Nevertheless, a more detailed comparison speaks in favor of the DRW description. Indeed, the fitting parameter $h_S^{(exp)} = 3 \pm 0.3$ and the cluster-fractal dimension $d_f^{(DRW)} = 1$ of the DRW model (see, respectively, Fig. 5 and Table 1) are supported by the experimental verification made in Figs. 1 and 2 for polymers in [56], which provided $d_f^{(pol)} = 1.00 \pm 0.09$. Below we specify an application of the DRW approach.

The model prediction (36), which now reads as

$$z^{(DRW)} = 3\left(\frac{1}{\beta}-1\right) = 2\left(\frac{1}{b}-1\right), \tag{41}$$

and restricted by

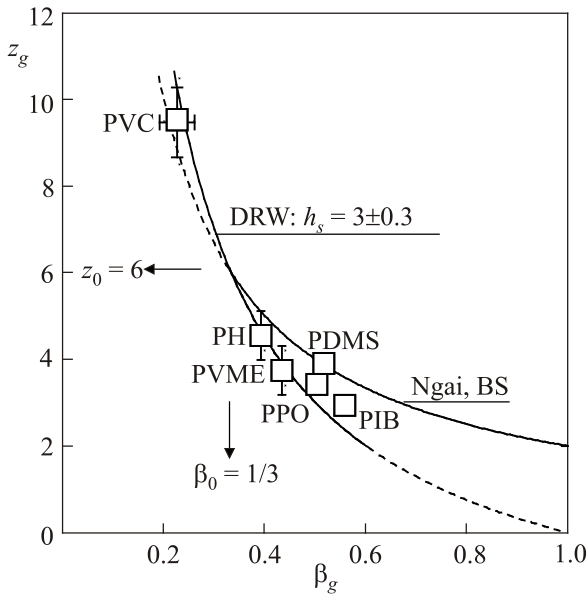$$z^{(DRW)} > 2; \quad \beta < 3/5 \text{ and } b < 1/2, \tag{42}$$

Fig. 5. Diffusion exponent against stretching exponent. The points are the quasi-elastic neutron scattering and fragility data reported for polymers in Refs. 6, 66, 67. The solid line DRW is drawn through the equation $(z_g + h_S)\beta_g = h_S$ (36), with $h_S = 3$, and the line Ngai [6] and Bendler–Shlesinger (BS) [68] — through $z_g\beta_g = 2$. The dashed lines indicate regions in which the models do not work. The model-crossover point $z_0 = 6$, $\beta_0 = 1/3$ is shown.

suggests a single α-relaxation mechanism. As given in Eqs. (41), it is described by subdiffusion exponent z_T, which is the same for the slow, fast, and presumably *intermediate* dynamics.

Instead of the two-cluster-type relaxation rationalized through the DRW description, a single-cluster consideration is generally considered. Examples are the modelling of the KWW relaxation by fractal-space coupling [6] or defect diffusion [68]. Both theories suggest the constraint $z = 2/\beta$ formally corresponding to the RWs on a high-dimensional critical percolation lattice in Euclidean space [69]. As proved [70], this percolation approach is bounded by the critical exponent $\beta_0 = 1/3$, earlier established in simulations of spin glasses [72]. It was also claimed [73], that the description of the primary relaxation in glass-forming polymers, constrained by $z\beta = 2$, diverges below and close to $\beta \approx 1/3$. As illustrated in Fig. 5, this critical point transforms, within the DRW model, into the *crossover point* described by the exponents

$$b_0 = \frac{1}{4}, \quad \beta_0 = \frac{1}{3} \text{ and } z_0 = 6, \tag{43}$$

following from Eq. (41). This enables one to shed a light on the structural relaxation in extremely fragile glass formers.

In contrast to SCLs, the possibility to approach the dynamical experimental data for polymers and networks by the same curve (shown by the solid line in Fig. 5) encouraged us to apply the DRW model to networks. Taking into account

the experimental data $0.50 \leq \beta_g^{(netw)} \leq 0.70$. One can expect that this subdiffusion relaxation must fail in silicas, plastic crystals, and other networks with $\beta_g^{(netw)} \geq 0.60$, as follows from (42). In these materials, a *superdiffusive* late-time relaxation given by the CTRW prediction, namely

$$z_g^{(CTRW)} = 2 - \frac{1}{\beta_g}, \tag{44}$$

follows from Eq. (33) and $h_S^{(CTRW)}$ presented in Table 1. In view of the fact that many neighbor steps are not available and therefore a random walker returns to the starting point, the CTRW prediction (44) is not appropriate for the "cage effect" description. It is not the case of SCLs near the α–β-bifurcation temperature T_c, where long-distance molecules jumps, controlled by random fields were observed through the CTRW model [65]. In the lithium-doped silicates, the CTRW relaxation regime was simulated [71] at frequencies near τ_c^{-1}. As far as the author knows, no experimental data on the diffusion exponent, clarifying the primary relaxation mechanism in SCLs near T_g and T_c, are available.

3.5. Relaxation mechanisms in orientational glasses

According to careful studies of melt polymers conducted in [4], the coarsed-grained *microscopic models* fail to describe correct dynamic behavior near T_g. In contrast, in structurally disordered orientational glasses (OGs) the mechanism of collective formation of the short-range orientational order is described in details. It is striking that, similarly to glass-forming polymers, where the structural relaxation is shown to be driven by unspecified *mesoscopic* random fields (DRW), a stabilization of the orientational order parameter in OG formers was proved [74–76] to be controlled by intrinsic local random fields. This *microscopic* level description in OGs, was not yet confronted with the mesoscopic-level modelling of the primary relaxation.

In general, OG metastable states emerge when dipolar or quadrupolar molecules under cooling avoid their long-range orientational order. Within the entire family of glass formers, OGs belonging to the class of networks [49], can be divided into two groups. The group of *plastic crystals* is often considered [77] as an ideal pattern for the pure OG state, which, unlike the group of the structurally disordered OGs formed by mixed and doped molecular crystals, is not affected by vibrations of the regular crystalline lattice. In other words, the site-disorder effects are absent in the plastic crystal group. In order to qualify the development of formation of metastable states with distinct degree of site-coupling and bond-coupling disorder, we introduce a conventional lattice-coupling parameter [79]

$$K = \frac{\text{orientational-positional interaction energy}}{\text{molecular orientational energy}}. \tag{45}$$

The group of plastic crystals with $K = 0$ is exemplified here by cyclo-octanol, cyclo-hexanol, and cyanoadamantane (CNA) [77,78]. OG materials with a weak orientational-vibrational coupling, and thus small K, are given [79] (i) by the dipolar spin glasses, where the spin-lattice coupling is commonly safely excluded, and (ii) by the quadrupolar-quantum and quadrupolar-classical glasses, exemplified by (i) potassium tantalate crystals doped by the off-center displaced ions (type of $KTaO_3$:Li and KCl:OH), (ii) ortho-para-hydrogen quantum (OPH, p-H_2:o-H_2), and argon-nitrogen classical (Ar:N_2) crystal mixtures formed by solidified solutions of spherical and linear, rotor-like quadrupolar molecules. OGs with relatively large K are the mixed cyanides (KBR:CN), rubidium ammonium dehydrogen phosphates (RADP, RbH_2PO_4:NH_4), and mixed betaine compounds (BPI, BP:BPI). With gradual increase in parameter K, one can expect the dynamical behavior to approach that in canonical structural glasses, such as SCLs, in which positional and rotational degrees of freedom are indistinguishable. They are designated, qualitatively, by $K = 1$. Review and analysis of experimental data in OG formers strongly corroborate the idea that dynamical slowing-down and correlation-length growth behavior set the trend during freezing into the OG state [79,80].

Unlike the cases of SCLs, OGs admit a Hamiltonian approach (see, e.g., [81,82]). Descriptions based on dynamic and thermodynamic microscopic models have been proposed for the *quadrupolar orientational glass* (QG) studied, respectively, in mixed cyanides [83,84], RADP crystals [74,85], and OPH mixtures [76]. By generalizing outputs of *microscopic models* developed for QGs, one can characterize the OG freezing mechanism as follows. A cooperative freezing of the orientational degrees of freedom is driven by random bond-type, highly frustrated coupling that dominates over intrinsic local-cite random fields, which are conjugated to and correlated with the local orientational order parameter. What is common for all OGs, both dipolar and quadrupolar, except for the group of plastic crystals, the bond and site randomness are originated from the site-substitutional disorder. When this disorder exceeds a certain level, the glass transformation process loses its cooperative character [74,81,83,86].

Starting from application of the DRW approach to the network glass formers, we now specify it for the case of OGs. A comparative behavior of relaxing units in structural and orientational slowing-downing is analyzed in Fig. 6.

As established in Fig. 6 by solid lines, the material-independent parameter m_β^* in Eq. (39) is well observable in certain classes of the glass-forming materials, where K (45) is large. These are strong-glass polymers (with $m_g^{(pol)} < 100$) and alcoholic SCLs. With concern to the networks tabulated in [49], the corresponding dynamical parameters $m_\beta^{(OG)}$ and $m_\beta^{(PC)}$ are also defined for both the groups of OGs distinguished through the parameter K. As is evident from Fig. 6, the dynamic behavior of OGs with
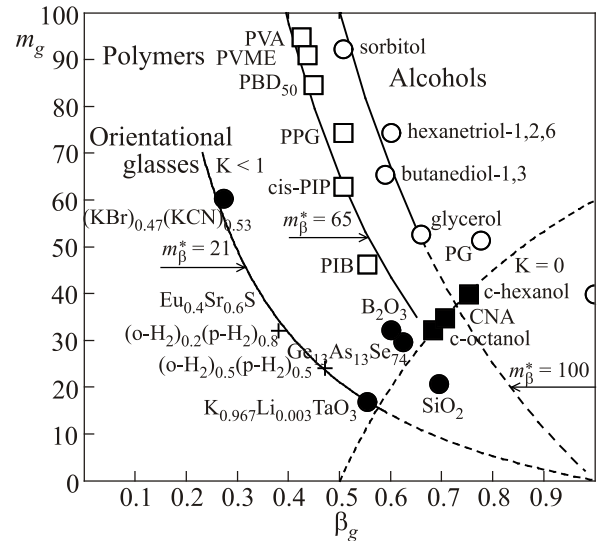

Fig. 6. Non-Arrhenius against non-Debye dynamical characteristics in orientational glass and other glass formers. Symbols are experimental data for alcoholic (circles) and polymeric (squares) liquids, both taken from Ref. 49; for OGs, formed by mixed and doped crystals (closed circles), including OPH (crosses) and plastic crystals (closed squares), taken from Table 2. The solid lines are drawn through the fragility $m_g = m_\beta^*(1/\beta_g - 1)$ (39) for OGs with $m_\beta^{(OG)} = 21$; for polymers with $m_\beta^{(pol)} = 65$ and for liquids with $m_\beta^{(liq)} = 100$. The thick dashed lines extrapolate domains of the DRW model. Plastic crystals fit by $m_g = m_\beta^{(PC)}(2 - 1/\beta_g)$, with $m_\beta^{(PC)} = 60$, shown by the thin dashed line. The conventional lattice-coupling parameter (45) is shown for mixed and doped crystals ($K < 1$) as well as for plastic crystals ($K = 0$).

$K = 0$ conflicts with that for $K \neq 0$, which behavior in turn is similar to that in the $K = 1$ representatives.

As follows from the analysis in Fig. 6, in all the studied structurally disordered materials with $K \neq 0$, the high-frequency part of the susceptibility provides direct observation of the trend to the long-time (cooperative) *structural correlations* growing with decreasing temperature. In these materials, the correlations are shown to be associated with the RW clusters which establish the *intermediate* cooperative scale given by $R_T = \langle R^2 \rangle_{RW}^{1/2}$ (20). In the structurally ordered plastic crystals, not obeying equation $m_g = m_\beta^*(1/\beta_g - 1)$, this correlation scale does not exist. Instead of R_T, the orientational degrees of freedom likely establish another relaxation scale, related to the *thermodynamic* average of molecular orientational fluctuations from the local equilibrium axes $\Omega_T = \langle \Omega^2 \rangle_T^{1/2}$. This scale is expected to be formed by the late-time correlations in orientational motion of dipoles (or quadrupoles) frozen near the axes determined by the condition $\langle \Omega \rangle_T = 0$. In this way, Ω_T plays the role of R_T. This suggests for the plastic crystals:

$$m_g = m_\beta^{(PC)}\left(2 - \frac{1}{\beta_g}\right) \text{ and } \beta_g > \frac{1}{2}, \qquad (46)$$

obtained by the fitting (shown in Fig. 6) to the data on $\beta_g^{(exp)}$ available from the literature and accumulated in Table 2.

In Table 2, the observed primary relaxation in OGs is parametrized through the VFT and KWW phenomenological forms. In line with Ref. 79, these materials are treated as regular strong-glass representatives of the glass-forming family. An exceptional behavior of OGs has been highlighted in Ref. 49, where the significant deviations from the correlated non-Debye and non-Arrhenius behavior were established phenomenologically [49] in all the studied glass formers (shown by the dashed line in Fig. 1 in Ref. 56). In what follows, we demonstrate that these deviations do not exceed the typical experimental error, if evaluated within the framework, consistent with the DRW model.

First, we found that for all types of OGs with $K \neq 0$ including spin glasses, the universal parameter $m_g^{(OG)} = 15$ established through Eq. (12) is within the typical error given by the domain $14 \leq m_g^* \leq 18$. The same refers to OGs with $K = 0$, for which $m_g^{(PC)} = 14.5$ is found. These results provide estimates for the Vogel temperature T_0 in those cases when T_0 is not available. In the next step, we have tested the predicted stretching exponent $\beta_g^{(KWW)}$, given in Eq. (40), which is consistent with Eq. (38), as shown through the two-cluster DRW modeling (41). The parameter $m_\beta^{(OG)} = 21$ is found through the fitting analysis of the observed stretching exponent $\beta_g^{(exp)}$, presented in Fig. 6. This analysis is associated with the observation of late-time relaxation dynamics in OGs, driven by random fields and caused by structural disorder. As the result, the material-independent parameter $m_z^{(OG)} = 7$ follows from Eq. (39), when $h_S^{(DRW)} = d_g = 3$ and $m_\beta^{(OG)} = 21$ are taking into account. We recall that the DRW consideration is limited by the Brownian regime diffusion, given by the *critical* exponents $z_{cr}^{(DRW)} = 2$ and $\beta_{cr}^{(DRW)} = 3/5$, in Eq. (42). Remarkably that $\beta = 3/5$ was obtained in both molecular dynamic simulations (of polymers, alloys, and soft sphere mixtures) and predicted by trap model [11].

Adopting the Brownian diffusion as the critical regime for any subdiffusion dynamics, considering in the space of effective dimension $d_g^{(PC)} = 6$, along with $m_z^{(PC)} = 10$, a plastic crystals:

$$z_g^{(PC)} = 6\left(2 - \frac{1}{\beta_g}\right) \text{ and } \beta_g \geq \frac{3}{5}, \qquad (47)$$

immediately follows from the experimentally observed Eqs. (46) and (39). Even though the suggested relaxation

Table 2. Parametrization of the primary relaxation timescale in orientational-glass materials

Glass formers	m_g	T_g, K	$\beta_g^{(exp)}$	$\beta_g^{(b)}$	T_0, K	$z_g^{(c)}$	Reference
$(BP)_{0.4}(BPI)_{0.6}$, odg	14.2	7.7	$35^{[74]}_{\pm 0.04}$	–	–	–	[49]
$K_{0.967}Li_{0.033}TaO_3$, odg	16.8	67	0.55	0.56	$7.2^{(a)}$	2.4	[49]
$K_{0.974}Li_{0.026}TaO_3$, odg	$17^{(a)}_{\pm 2}$	50	–	0.55	6.0	2.4	[79]
$(o\text{-}H_2)_{0.5}(p\text{-}H_2)_{0.5}$, oqg	$23_{\pm 2}$	$52_{\pm 0.03}$	$0.48_{\pm 0.02}$	0.48	0.16	3.3	Fig. 7
$Rb_{0.65}(NH_4)_{0.35}H_2PO_4$, odg	27	17.6	–	0.44	$10^{[80]}$	3.9	[49]
$(o\text{-}H_2)_{0.2}(p\text{-}H_2)_{0.8}$, oqg	$33_{\pm 3}$	$0.45_{\pm 0.04}$	$0.40_{\pm 0.02}$	0.39	0.22	4.7	Fig. 7
$C_8H_{15}OH$ (c-octanol), pc	33	168	0.70	0.69	94.7	3.3	[77]
$C_8H_{15}CN$ (CNA), pc	35	177	0.70	0.71	$104^{(a)}$	3.5	[49]
cyclo-hexanol, pc	40	$153^{(a)}$	0.75	0.75	97.5	4.0	[77]
$Eu_{0.40}Sr_{0.60}S$, sg	$39^{(b)}_{\pm 9}$	1.9	$0.34_{\pm 0.05}$	0.35	$1.2^{(a)}$	5.6	[87]
$Rb_2Cu_{0.78}Co_{0.22}F_4$, msg	47	3.6	–	0.31	$2.5^{(a)}$	6.7	[49]
$KBr_{0.47}KCN_{0.53}$, oqg	60	64	0.27	0.26	$48^{(a)}$	8.6	[49]
$(C_2F_6)_{0.68}(CClF_3)_{0.32}$, oqg	93	41.3	–	0.18	$35^{(a)}$	13	[49]

Notations are given for orientational dipolar (odg) and orientational quadrupolar (oqg) glasses; plastic crystals (pc), metallic (msg) and non-metallic (sg) spin glasses.

(a) Estimated through Eq. (9) with $m_g^{(OG)} = 15$ for all studied materials, except for plastic crystals, where $m_g^{(PC)} = 14.5$ is adopted.

(b) Estimated through Eq. (40) with $m_\beta^{(OG)} = 21$. For plastic crystals estimated through by $\beta_g^{(PC)} = m_\beta^{(PC)}/(2m_\beta^{(PC)} - m_g)$, with $m_\beta^{(PC)} = 60$, first established in Ref. 65.

(c) Estimated through $z_g = m_g/m_z^*$ (38), $m_z^{(OG)} = 7$, and $m_z^{(PC)} = 10$.

regime (47) is not classified in Table 1, it can be compared with Eq. (44) expected for the CTRW model and corresponding to the effective space $d_g^{(CTRW)} = 1$. Moreover, Eq. (47) does not conflict with the model-independent instability of the DRW primary relaxation in the structural-disordered OGs established by the limit $K \to 0$. This limit corresponds to the effective weakening of lattice-coupling interaction and is supported by estimations, provided below for QG in $(o\text{-}H_2)_x (p\text{-}H_2)_{1-x}$ mixtures with $x \to x_{max}$ and anticipated in Fig. 6.

Apart from the theoretical estimates, the experimental testing of the proposed mechanisms of the slowing-down of structural and orientational rearrangements is associated with the observation of material-independent quantities $m_z^{(OG)} = 7$ and $m_z^{(PC)} = 10$, expected in, respectively, *site-substituted* and *bond-frustrated* OG forming materials. In Fig. 7 the proposed diffusion regimes are plotted for those materials, in which the KWW relaxation was experimentally observed.

Finally, a subdiffusion primary relaxation in non-polymeric liquids, namely, in SCLs:

$$z_g^{(SCL)} = 6\left(\frac{1}{\beta_g} - 1\right) > 2 \qquad (48)$$

was proposed in Eq. (47) in Ref. 17. This mechanism corresponds to the DRW diffusive dynamics developing in the space of dimension $d_g^{(SCL)} = 6$. Again, considering the normal diffusion as the critical limit, one finds from Eq. (48) that $\beta_g < \beta_{cr}^{(SCL)} = 3/4$ that is in agreement with the experimental data discussed in Ref. 56.
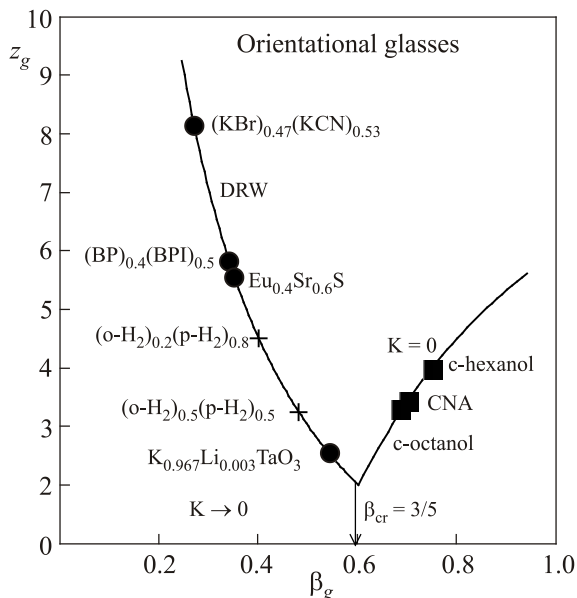

Fig. 7. Theoretical predictions for the primary relaxation regimes in orientational glasses: diffusion exponent against stretching exponent. The solid lines are given by Eqs. (41) and (47) for OGs with $K \neq 0$ and $K = 0$, respectively. Symbols (circles) are drawn through the same equations and shown for materials with the known data on $\beta_g^{(exp)}$, presented in Table 2. The DRW instability limit is also shown through the lattice-coupling parameter K (45).

4. Summary

We have reviewed the problem of primary structural relaxation in a number of glass-forming materials presented by molecular and polymeric supercooled liquids, metallic alloys, and orientational-glass crystals, including plastic crystals. It has been demonstrated that such a generalized way of treatment of the glass-formation process in microscopically different systems is possible, if designed on a mesoscopic level. Although a unique coherent theoretical framework remains a challenge, the proposed complex geometric, dynamic and thermodynamic approach to the problem offers novel relations between the observable dynamical exponents and thermodynamic and kinetic parameters, which shed light onto the universal features underlying temporal-spatial correlations in the primary relaxation of glass formers. A macroscopic parametrization of the primary timescale, done in a self-consistent manner, provides strong evidence for mutual dependence between thermodynamic (T_0 and T_g) and dynamic (T_c) characteristic temperatures. The exclusion of material-dependent parameters results in the universal CTE, which is proved to be valid to those glass formers, for which all the three temperatures are available from the literature.

The late-time anomalous Debye behavior is "geometrically" mapped onto the effective relaxation space of dimension d, which is thought as to be ultimately related to a number of independent (unspecified) dynamical variables. Near and above the structural arrest temperature T_g, the dimension $d_g^{(pol)} = 3$ is derived in glass-forming polymers, whose entangled-chain structure is observed through the large clusters of fractal dimension $d_f^{(pol)} = 1$. Similarly, the dimension $d_g^{(QG)} = 3$ is expected in quadrupolar-glass formers [56]. This case is described by the ensemble of percolative rotor-like clusters, for which $d_f^{(QG)} = 5/2$ is derived in the metastable state in ortho-para hydrogens. In molecular SCLs, where the relaxing units emerge as dense, solid-like clusters of dimension $d_f^{(liq)} = d = 3$, the effective space of relaxation of dimension $d_g^{(liq)} = 6$ is due to the compatibility of the primary relaxation scale with the VFT form [17]. As proven for a certain class of glass formers, the cluster-shape parameter d_f is a material independent regardless of the underlying microscopic chemical structure. Moreover, the found in dynamic experiments dimension $d_g = 6$ is expected to be the same in all simple, complex, and alcoholic liquids, as well as in plastic crystals; whereas $d_g = 3$ is proved for polymeric liquids and is expected for all orientational-glass materials formed by mixed and doped crystals. Within the framework of dynamic stochastic approach, the corresponding universal relaxation mechanism, DRW, is ensured and identified by self-similarity of percolative-type clusters.

A mesoscopic-level relaxation scenario is developed through the dynamic and thermodynamic statistic descriptions. The structural relaxation was described within the two-cluster scheme of the two asymptotic scaling laws: the short-time von Schweidler law and the late-time KWW law. The universal features of the α-relaxation were stipulated by slow growth of correlations, under cooling, as well as by the self-similarity of the mesoscopic-scale hierarchical structure of these correlations. If the specification of correlations depends on the chosen theoretical scheme, their structure similarity is manifested through the existence of weakly material-dependent parameters, which link between the dynamical exponents and thermodynamic parameters in glass formers.

Above T_c, the mechanism of structural relaxation, associated with the formation of ML-clusters in SCLs [43] and that of the percolative-like clusters in Li-doped networks [71], is due to random jumps in effective relaxation space realized on temporal fractals. Further study is required to find out whether the relevant CTRW mechanism is generic for other glass formers, at α–β-bifurcation temperature T_c. To a certain extent, the related problem is elucidated near T_g, where the DRW universal relaxation mechanism is established. It is shown here that in all materials with a quenched structural disorder, such as SCLs, mixed and doped non-metallic crystals, and metallic alloys the subdiffusive cluster dynamics occurs through random walks on spatial fractals, driven by random fields. This structural-arrest is observed through the DRW mechanism in polymeric-glass and orientational-glass materials, but it is also expected to be valid in SCLs.

Unlike the "static" parameter d_g, which is a constant in a given class of glass formers, the slow dynamical exponent β_g and the subdiffusion exponent z_g are determined by the underlying chemical structure. The same refers to macroscopic timescale characteristics, such as expansivity [56], fragility m_g, and curvature (second derivative time-scale [17]), for which novel relations are proposed on the basis of weakly-material-dependent parameters. By choosing m_g as an external parameter accessible in both dynamic [49] and thermodynamic [88] experiments, the domains $1/2 \leq \beta_g^{(\mathrm{liq})} \leq 3/4$ and $1/2 \leq \beta_g^{(\mathrm{pol})} \leq 1/4$ are experimentally distinguished in all SCLs and polymers. These domains eventually diversify subdiffusive regimes of structural relaxation. Being governed by the same DRW cluster dynamics, the primary relaxation in non-polymeric and polymeric glass-forming liquids is correspondingly bounded as $2 \leq z_g^{(\mathrm{liq})} \leq 6$ and $3 \leq z_g^{(\mathrm{pol})} \leq 9$. The non-polymeric glass formers need though further experimental verification.

In view of that mesoscopic clusters modify their characteristics in space and time during glass formation, they were denominated [17] heterostructured clusters. Meanwhile, they preserve their self-similarity, which regardless of microscopic realizations and the chosen scheme of description, ensures universal features in primary structural relaxation manifested near the dynamic crossover temperatures T_c and T_e. The latter indicates a failure of the dynamic-thermodynamic ergodic description corroborated by the NMR data on the dynamic instability in molecular liquids, polymers, and metallic alloys. The two-version relaxation scheme elaborated for the description of ergodic-non-ergodic dynamic crossover revealed that at T_e is located always below and close to T_g [89]. A novel cluster ergodic-nonergodic description near T_e yielded a new tool for accounting for a number local-equilibrium states in Goldstein's energy landscape [90].

Acknowledgments

1. P.G. Debenedetti and F.H. Stillinger, *Nature* **410**, 259 (2001).
2. C.A. Angell, K.L. Ngai, G.B. McKenna, P.F. McMillan, and S.W. Martin, *J. Appl. Phys.* **88**, 3113 (2000).
3. W. Götze and L. Sjögen, *Rep. Prog. Phys.* **55**, 241 (1992).
4. K. Binder, J. Baschnagel, and W. Paul, *Prog. Polym. Sci.* **28**, 115 (2003).
5. K.L. Ngai, R.W. Rendell, and D.J. Plazek, *J. Chem. Phys.* **94**, 3018 (1991).
6. K.L. Ngai, In: *Disorder Effects on Relaxation Processes: Glasses, Polymers, Proteins*, R. Richert and A. Blumen (eds.), Springer, Berlin (1994).
7. J. Jäckle, In: *Disorder Effects on Relaxation Processes: Glasses, Polymers, Proteins*, R. Richert and A. Blumen, (eds.), Springer, Berlin (1994).
8. A. Hunt, *J. Phys.: Condens. Matter* **6**, 8087 (1994).
9. R.V. Chamberlin, *Phys. Rev. B* **48**, 15638 (1993).
10. R.V. Chamberlin, *Europhys Lett.* **33**, 545 (1996).
11. J.C. Phillips, *Rep. Prog. Phys.* **59**, 1133 (1996).
12. J.T. Bendler, J.J. Fontanella, and M.F. Shlesinger, *Phys. Rev. Lett.* **87**, 19 (2001).
13. A.S. Bakai, *Fiz. Nizk. Temp.* **20**, 469, 477 (1994) [*Low Temp. Phys.* **20**, 373, 379 (1994)].
14. A.S. Bakai, *Fiz. Nizk. Temp.* **22**, 956 (1996) [*Low Temp. Phys.* **22**, 733 (1996)]; *ibid.* **24**, 27 (1998) [**24**, 20 (1998)].
15. A.S. Bakai and E.W. Fischer, *J. Chem. Phys.* **120**, 5235 (2004).
16. V.B. Kokshenev, *Solid State Commun.* **119**, 429 (2001).
17. V.B. Kokshenev, P.D. Borges, and N.S. Sullivan, *J. Chem. Phys.* **122**, 114510 (2005).
18. V.B. Kokshenev, *Phys. Rev. E* **57**, 1187 (1998).
19. J.H. Gibbs and G. Adam, *J. Chem. Phys.* **43**, 139 (1965).
20. W. Kauzmann, *Chem. Rev.* **43**, 219 (1948).
21. R. Richert and C.A. Angell, *J. Chem. Phys.* **108**, 9016 (1998).
22. C.A. Angell, *J. Non-Cryst. Solids* **131–133**, 13 (1991).
23. M. Wolfgardt, J. Baschnagel, W. Paul, and K. Binder, *Phys. Rev. E* **54**, 1535 (1996).
24. C.A. Angell, *Physica D* **107**, 122 (1997).
25. T. Odagaki, *Phys. Rev. Lett.* **75**, 37 (1995).
26. U. Mohanty, G. Diezemann, and J.T. Fourkas, *J. Chem. Phys.* **113**, 3719 (2000).

27. V.N. Novikov and A.P. Sokolov, *Phys. Rev. E* **67**, 031507-1 (2003).
28. M. Goldstein, *J. Chem. Phys*. **51**, 3728 (1969).
29. R. Rössler, *Phys. Rev. Lett*. **65**, 1595 (1990).
30. C. Hansen, F. Stickel, T. Berger, R. Richert, and E.W. Ficher, *J. Chem. Phys*. **107**, 1086 (1997).
31. R. Schilling, In: *Disorder Effects on Relaxation Processes: Glasses, Polymers, Proteins*, R. Richert and A. Blumen (eds.), Springer, Berlin (1994).
32. F. Stickel, E.W. Fischer, and R. Richert, *J. Chem. Phys*. **102**, 6251 (1995).
33. F. Stickel, E.W. Fischer, and R. Richert, *J. Chem. Phys*. **104**, 2043 (1996).
34. E. Rössler and A.P. Sokolov, *Chem. Geol*. **128**, 143 (1996).
35. C.A. Angell, *J. Chem. Phys*. **49**, 863 (1988).
36. C.A. Angell, *Science* **267**, 1924 (1995).
37. A.P. Sokolov, W. Steffen, and E. Rössler, *J. Phys.: Condens. Matter* **8**, 9587 (1996).
38. M. Fuchs, W. Götze, S. Hidebrand, and A. Latz, *J. Phys.: Condens. Matter* **4**, 7707 (1992).
39. J.T. Bendler and M.F. Shlesinger, *J. Stat. Phys*. **53**, 531 (1988).
40. J. Souletie, *J. Phys. France* **51**, 883 (1990).
41. R.V. Chamberlin, *Phys. Rev. Lett*. **82**, 2520 (1999).
42. M. Mézard and G. Parisi, *Phys. Rev. Lett*. **82**, 747 (1999).
43. V.B. Kokshenev and N.S. Sullivan, *J. Low Temp. Phys*. **122**, 413 (2001).
44. R.H. Colby, *Phys. Rev. E* **61**, 1783 (2000).
45. D. Kivelson, G. Tarjus, X. Zhao, and S.A. Kivelson, *Phys. Rev. E* **53**, 751 (1996).
46. V.B. Kokshenev, In: *Atomic and Molecular Cluster Research*, F. Columbus (ed.), Nova Science Publishers Inc. N.Y. (2006).
47. V.B. Kokshenev, *Physica A* **262**, 88 (1999).
48. R. Böhmer and C.A. Angell, *Phys. Rev. B* **48**, 5857 (1993).
49. R. Böhmer, K.L. Ngai, C.A. Angell, and D.J. Plazek, *J. Chem. Phys*. **99**, 4201 (1993).
50. M. Tatsumisago, B.L. Halfpap, J.L. Green, S.M. Lindsay, and C.A. Angell, *Phys. Rev. Lett*. **64**, 1549 (1990).
51. R. Böhmer and C.A. Angell, *Phys. Rev. B* **45**, 10 091 (1992).
52. Y. Zhao, X. Bian, K. Yin, J. Zhou, J. Zhang, and X. Hou, *Physica B* **349**, 327 (2004).
53. R.V. Chamberlin, R. Böhmer, E. Sanchez, and C.A. Angell, *Phys. Rev. B* **46**, 5787 (1992).
54. J. Gerardin, S. Mohanty, and U. Mohanty, *J. Chem. Phys*. **119**, 4473 (2003).
55. V.N. Novikov, E. Rössler, V.K. Malinovsky, and N.V. Surovtsev, *Europhys. Lett*. **35**, 289 (1996).
56. V.B. Kokshenev, *Fiz. Nizk. Temp*. **33**, 805 (2007) [*Low Temp. Phys*. **33**, 617 (2007).
57. B.I. Halperin and P.C. Hohenberg, *Phys. Rev*. **117**, 952 (1969).
58. H.E. Stanley, In: *Scaling Phenomena in Disordered Systems*; R. Pynn and A. Skjeltorp (eds.), Plenum Press, New York and London (1985).
59. A.J. Bray, *Adv. Phys*. **43**, 357 (1994).
60. P.K. Dixon, L. Wu, S.R. Nagel, B.D. Williams, and J.P. Carini, *Phys. Rev. Lett*. **65**, 1108 (1990).
61. D. Stauffer and A. Aharony, *Introduction to Percolation Theory*, Taylor and Francis (eds.), London (1992).
62. M.B. Isichenko, *Rev. Mod. Phys*. **64**, 961(1992).
63. G. Zumofen, J. Klafter, and A. Blumen, In: *Disorder Effects on Relaxation Processes: Glasses, Polymers, Proteins*, R. Richert and A. Blumen (eds.), Springer, Berlin (1994).
64. M.E. Fisher, *J. Chem. Phys*. **44**, 616 (1966).
65. V.B. Kokshenev and N.S. Sullivan, *Phys. Lett. A* **208**, 97 (2001).
66. J. Colmenero, A. Alegria, A. Arbe, and B. Frick, *Phys. Rev. Lett*. **69**, 478 (1992).
67. J. Colmenero, *Physica A* **201**, 38 (1993).
68. J.T. Bendler, J.J. Fontanella, and M.F. Shlesinger, *Chem. Phys*. **284**, 311 (2002).
69. S. Alexander and R. Orbach, *J. Phys. Lett*. **43**, 625 (1982).
70. R.M.C. Almeida, N. Lemke, and I.A. Campbell, *J. Magn. Magn. Matter* **226**, 1296 (2001).
71. J. Habasaki and Y. Hiwatari, In: *Slow Dynamics in Complex Systems;* M. Tokuama, Oppenheim, Vol. I, Eighth Tohwa University International Symposium, AIP (1999).
72. I.A. Campbell and L. Bernardi, *Phys. Rev. B* **50**, 12643 (1999).
73. A. Alegra, J. Colmenero, P.O. Mari, and I.C. Campbell, *Phys. Rev. E* **59**, 6888 (1999).
74. R. Blinc, T. Apih, J. Dolinšek, M. Šprogar, and B. Zalar, *Phys. Rev. B* **52**, 15217 (1995).
75. F.F. Haas, K. Volmayr, and K. Binder, *Z. Phys. B* **99**, 393 (1996).
76. V B. Kokshenev, *Phys. Rev. B* **53**, 2191 (1996).
77. D.L. Leslie-Pelecky and O.P. Birge, *Phys. Rev. Lett*. **72**, 1232 (1994); *Phys. Rev. B* **18**, 13250 (1994).
78. R. Brand, P. Lukenheimer, U. Schneider, and A. Loidl, *Phys. Rev. Lett*. **82**, 1951 (1999).
79. U.T. Höchli, K. Knorr, and A. Loidl, *Adv. Phys*. **39**, 405 (1990).
80. A. Loidl and R. Böhmer, In: *Disorder Effects on Relaxational Processes: Glasses, Polymers, Proteins*, R. Richert and A. Blumen (eds.), Springer, Berlin (1994).
81. A.B. Harris and H. Meyer, *Canad. J. Phys*. **63**, 3 (1985).
82. K. Binder and J.D. Reger, *Adv. Phys*. **41**, 547 (1992).
83. C. Bostoen and K.H. Michel, *Phys. Rev. B* **43**, 4415 (1991).
84. B. Tadc, R. Pirc, and R. Blinc, *Phys. Rev. B* **55**, 816 (1997).
85. R. Pirc, B. Tadc, and R. Blinc, *Physica A* **185**, 322 (1992); *Phys. Rev. B* **36**, 8607 (1987).
86. V.B. Kokshenev, *Solid State Commun*. **55**, 143 (1985); V.B. Kokshenev and A.A. Litvin, *Fiz. Nizk. Temp*. **13**, 430 (1987) [*Sov. J. Low Temp. Phys*. **13**, 195 (1987)].
87. I.A. Campbell, J.M. Flesselles, R. Jullien, and R. Botet, *Phys. Rev. B* **37**, 3825 (1988).
88. L.M. Wang, V. Velikov, and A.J. Angell, *J. Chem. Phys*. **117**, 10184 (2002).
89. V.B. Kokshenev, *Fiz. Nizk. Temp*. **37**, 551 (2011) [*Low Temp. Phys*. **37**, 439 (2011)].
90. V.B. Kokshenev, *Fiz. Nizk. Temp*. **35**, 371 (2009) [*Low Temp. Phys*. **35**, 282 (2009)].